Biophys Rep 2024, 10(5):336–348
https://doi.org/10.52601/bpr.2024.240015

Biophysics Reports

RESEARCH ARTICLE

Special Topic - CALCIUM SIGNALING

The rectification of heterotypic Cx46/Cx50 gap junction channels depends on intracellular magnesium

Honghong Chen[1], **Donglin Bai**[1] ✉

[1] Department of Physiology and Pharmacology, University of Western Ontario, London, Ontario, Canada

Received: 24 March 2024 / Accepted: 10 July 2024

Abstract Gap junction (GJ) intercellular communication is crucial in many physiological and pathological processes. A GJ channel is formed by head-to-head docking of two hexameric hemichannels from two neighboring cells. Heterotypic GJ channels formed by two different homomeric connexin hemichannels often display rectification properties in the current–voltage relationship while the underlying mechanisms are not fully clear. Here we studied heterotypic Cx46/Cx50 GJs at a single GJ channel level. Our data showed unitary Cx46/Cx50 GJ channel conductance (γ_j) rectification when 5 mmol/L Mg^{2+} was included in the patch pipette solution, while no γ_j rectification was observed when no Mg^{2+} was added. Including 5 mmol/L Mg^{2+} in pipette solution significantly decreased the γ_j of homotypic Cx46 GJ with little change in homotypic Cx50 γ_j. A missense point variant in Cx46 (E43F) reduced the Mg^{2+}-dependent reduction in γ_j of Cx46 E43F GJ, indicating that E43 might be partially responsible for Mg^{2+}-dependent decrease in γ_j of Cx46. A comprehensive understanding of Mg^{2+} modulation of GJ at the individual channel level is useful in understanding factors in modulating GJ-mediated intercellular communication in health and diseases.

Keywords Gap junction channel, Heterotypic gap junction, Rectification, Single channel analysis, Patch clamp

INTRODUCTION

Gap junctions (GJs) are clusters of intercellular channels that provide direct passage of ions, nutrients, metabolic wastes, and small signaling molecules between adjacent cells to regulate tissue/organ homeostasis (Goodenough and Paul 2009). A GJ channel is formed from two head-to-head docked connexons (known as hemichannels) and each connexon is composed of six connexins (Goodenough and Paul 2009). Twenty-one human genes and twenty mouse genes are identified to encode for connexins and all of the connexins share the same topological structures with four transmembrane domains (M1–M4), two extracellular loops (E1 and E2), one cytoplasmic loop (CL), and amino terminus (NT) and carboxyl terminus (CT) in the cytosol (Kumar and Gilula 1996). Connexin expression is tissue cell-specific, and each tissue cell often expresses one or more connexins, leading to the formation of homomeric homotypic, homomeric heterotypic, and/or heteromeric heterotypic GJs (Saez *et al.* 2003; Goodenough and Paul 2009). Depending on the component connexins, different GJs showed a variety of properties and can be modulated by many factors, including intracellular pH, transjunctional voltage (V_j), post-translational modifications, and intracellular divalent cations, such as Ca^{2+} and Mg^{2+} (Peracchia *et al.* 2000; Bukauskas and Verselis 2004; Lampe and Lau 2004; Bargiello and Brink 2009).

Early studies documented that elevation of intracellular Ca^{2+} concentrations (*i.e.*, $[Ca^{2+}]_i$) leads to GJ uncoupling in various cells (Loewenstein *et al.* 1967; Oliveira-Castro and Loewenstein 1971; Noma and Tsuboi 1987). Similar to this action of $[Ca^{2+}]_i$, $[Mg^{2+}]_i$ can also uncouple GJs at millimolar concentrations, which are much higher than those required for $[Ca^{2+}]_i$

✉ Correspondence: donglin.bai@schulich.uwo.ca (D. Bai)

to reduce GJ coupling (Oliveira-Castro and Loewenstein 1971; Peracchia and Peracchia 1980; Noma and Tsuboi 1987; Matsuda *et al.* 2010). More recent studies on recombinantly expressed connexins showed that the coupling conductance of the GJs formed by Cx26, Cx32, Cx36, Cx43, Cx45, or Cx47 were all reduced in 5 mmol/L $[Mg^{2+}]_i$ from the initial coupling level (Palacios-Prado *et al.* 2013). However, a much lower $[Mg^{2+}]_i$ (0.1–0.01 mmol/L) was found to enhance Cx36 GJ coupling conductance, but not other tested GJs (Palacios-Prado *et al.* 2013). This unique $[Mg^{2+}]_i$ modulation on Cx36 was mapped to the residue Asp47 (D47) of Cx36, which is at the border of M1 and E1 domains (Palacios-Prado *et al.* 2014). Interestingly, the border of M1 and E1 domains has been shown to be the site for Ca^{2+} binding in Cx26 GJs (E42, G45 and E47 of Cx26), and one of these residues (G45) is the equivalent residue of D47 of Cx36 (Bennett *et al.* 2016). Additionally, a Ca^{2+} binding site responsible for hemichannel gating was identified at the residues (E47 and D50) in Cx26 (Lopez *et al.* 2016) and also at the M1–E1 border region. The M1–E1 region in other connexins, including Cx46 and Cx50, are highly conserved and a cluster of three or more negatively charged residues were found to be the pore lining/accessible residues in the high-resolution structure models (Myers *et al.* 2018; Flores *et al.* 2020). Pore lumen accessibility and multiple negative charges in Cx46 and Cx50 GJs at this M1–E1 border region suggest that this domain may also be able to bind divalent cations, including Mg^{2+}. Functional study with different concentrations of $[Mg^{2+}]_i$ showed a dose-dependent reduction of the unitary channel conductance (γ_j) of Cx50 GJ (Tejada *et al.* 2018). However, it is not clear if $[Mg^{2+}]_i$ can modulate the γ_j of homotypic Cx46 or heterotypic Cx46/Cx50 GJs in a similar way.

The human eye lens is an avascular organ, and its development and transparency are dependent on microcirculations mediated by GJ networks (Mathias *et al.* 2010). Cx46, Cx50 and Cx43 are expressed in the lens with both Cx50 and Cx43 in the epithelial cells and the Cx46 and Cx50 in the lens fiber cells which make up the bulk of the lens (Beyer *et al.* 1989; Paul *et al.* 1991; White *et al.* 1992; Mathias *et al.* 2010). Over one hundred mutations in the genes encoding either Cx46 or Cx50 have been linked to congenital cataracts (Beyer *et al.* 2013; Bai *et al.* 2021). Many of these mutations are co-segregated with the disease for multiple generations (Beyer *et al.* 2013; Ceroni *et al.* 2019). Functional studies of these cataracts linked Cx46 or Cx50 mutants revealed a loss of GJ function as a common mechanism for these mutants (Pal *et al.* 1999; Tong *et al.* 2013; Schadzek *et al.* 2016; Abrams *et al.* 2018; Li *et al.* 2023). Consistent with these findings, the mouse models with either Cx46 or Cx50 genes knockout also developed cataracts (Gong *et al.* 1997; White *et al.* 1998) and mutations in mouse Cx50 gene also linked to inherited cataracts (Xu and Ebihara 1999; Berthoud *et al.* 2019). In summary, compelling evidence from genetic, functional, and animal models is accumulated for an important role of GJs formed by Cx46 and Cx50 for lens transparency.

Co-expression of Cx46 and Cx50 in the lens fiber cells opens the theoretical possibilities of forming different types of GJs (Mathias *et al.* 2010). Studies in native lens tissues revealed that heteromeric GJs with both Cx46 and Cx50 were formed (Konig and Zampighi 1995; Jiang and Goodenough 1996; Myers *et al.* 2018). Recombinant expression studies indicate that functional homomeric heterotypic Cx46/Cx50 GJs can be formed in model cells (White *et al.* 1994; Hopperstad *et al.* 2000; Wong *et al.* 2024). Here we studied homomeric heterotypic Cx46/Cx50 GJs at a single channel level to determine the γ_js under Mg^{2+}-free and added Mg^{2+} intracellular solutions. To align our functional study with the high resolution of sheep Cx46 and Cx50 GJ structure models (Myers *et al.* 2018; Flores *et al.* 2020), we used the sheep version of Cx46 and Cx50 to evaluate the effect of $[Mg^{2+}]_i$ on the γ_j of these GJs. Our results showed that the rectification property of heterotypic Cx46/Cx50 GJs depended on the presence of intracellular Mg^{2+}. This is likely due to a higher sensitivity of Cx46 GJ to $[Mg^{2+}]_i$. Studying the mechanisms of $[Mg^{2+}]_i$ modulation in these lens GJs may shed light on the divalent cation modulation of many GJs in health and disease conditions.

RESULTS

Cx46/Cx50 GJ showed rectification in the presence of Mg^{2+}

To study homomeric heterotypic Cx46/Cx50 GJ channels, we mixed cells expressing Cx46-IRES-DsRed with cells expressing Cx50-IRES-GFP and selected cell pairs with successfully expressing the fluorescent reporters, one red (DsRed+) and the other one green (GFP+) for dual whole-cell voltage clamp experiment. Transjunctional voltage (V_j) was generated by a series of voltage pulses delivered in one cell of the pair while holding the other cell of the pair constantly at zero to record transjunctional current. Cell pairs with only 1–2 functional GJ channels were selected for further analysis.

Representative unitary transjunctional currents (i_js) in response to a series of V_js are shown in Fig. 1 under Mg^{2+}-free intracellular solution (ICS). The i_js of the main conducting state were plotted with V_js and a linear regression of i_j–V_j plot was used to obtain slope single channel conductance (γ_j) for two current flow directions. The γ_j of Cx46+ (defined as relative +V_js on the Cx46-expressing cell comparing to the Cx50-expressing cell) was 208.4 ± 6.7 pS (n = 6), which is not significantly different from the γ_j (201.4 ± 4.8 pS, n = 6, P = 0.50) of Cx46– (relative –V_js on the Cx46 cell comparing to the Cx50 cell) in Mg^{2+}-free ICS. This is surprising considering a previous study reported rectification of heterotypic rodent Cx46/Cx50 GJ (Hopperstad *et al.* 2000). With a closer comparison of the experimental conditions, we found that the ICS in that study contained 3 mmol/L Mg^{2+}, which could modify the γ_j as reported in Cx50 GJ (Tejada *et al.* 2018). To test this possibility, we used ICS containing 5 mmol/L Mg^{2+} in the form of MgATP to repeat the previous experiment. With 5 mmol/L Mg^{2+} in ICS, we observed rectification for heterotypic Cx46/Cx50 GJ with the γ_j of Cx46+ (178.7 ± 4.8 pS, n = 6) which was significantly higher than the γ_j of Cx46– (147.8 ± 3.8 pS, n = 6, $^{**}P$ = 0.005, Fig. 1). Both Cx46+ and Cx46– γ_js in 5 mmol/L Mg^{2+} were lower than the corresponding γ_js in the absence of Mg^{2+} as indicated in Fig. 1C.

The γ_js of homotypic Cx46 GJs were decreased in the presence of intracellular Mg^{2+}

It is interesting to observe a $[Mg^{2+}]_i$-dependent rectification of heterotypic Cx46/Cx50 GJ channels. To explore the underlying mechanisms, we studied the γ_js of homotypic Cx46 and Cx50 GJs in the absence and presence of Mg^{2+}. As shown in Fig. 2, i_js of homotypic Cx46 and Cx50 GJs were recorded with Mg^{2+}-free and Mg^{2+}-containing (5 mmol/L) ICS. The slope γ_js were obtained by linear regression of i_j–V_j plot for each cell pair of these homotypic GJs and then plotted as a bar graph (Fig. 2 bottom panels). The γ_j of Cx46 GJ was 192 ± 5.1 pS (n = 5) in the absence of Mg^{2+}, which was significantly higher than the γ_j in the presence of 5 mmol/L Mg^{2+} (149 ± 3.9 pS, n = 4, $^{***}P$ < 0.001, Fig. 2). In other words, 5 mmol/L Mg^{2+} caused an average 22% reduction of the slope γ_j of Cx46 GJ. Different from Cx46 GJ, the γ_j of Cx50 GJ was 219 ± 5.3 pS (n = 5) in the absence of Mg^{2+}, which was not statistically different from the γ_j in the presence of 5 mmol/L Mg^{2+} (193 ± 11 pS, n = 5, P = 0.065, Fig. 2). Though an apparent decrease in the slope γ_j of Cx50 GJ in 5 mmol/L Mg^{2+} was observed (12%).

The 43rd residue in Cx46 GJ could be partially responsible for its Mg^{2+} modulation

To explore the underlying structural mechanism of Mg^{2+} modulation of Cx46 γ_j, we looked for sequence differences between Cx46 and Cx50 at a region identified to be important for divalent cation binding/modulation in other GJs, specifically Mg^{2+} modulation site in Cx36 and Ca^{2+}-binding site in Cx26 GJs (Palacios-Prado *et al.* 2014; Bennett *et al.* 2016). We first aligned these connexins at the region of E1–M1 domain region (Fig. 3A). The previously identified Ca^{2+}-binding residues (E42, G45, and E47) in Cx26 GJ overlaps with the key residue identified for Mg^{2+}-modulation in Cx36 (D47 which is aligned with G45 of Cx26) (Palacios-Prado *et al.* 2014; Bennett *et al.* 2016). Both Cx46 and Cx50 sequences in this region are highly homologous and aligned very well with either Cx26 or Cx36 (Fig. 3A). The only obvious difference was observed on the 43rd position (the equivalent residue in Cx26, E42, involved in binding Ca^{2+}) where in Cx46 was also a negatively charged glutamate (E43) whereas in Cx50 was a non-charged aromatic phenylalanine (F43). According to the high-resolution structures of Cx46 and Cx50 GJs (Myers *et al.* 2018; Flores *et al.* 2020), the 43rd residue in Cx46 and Cx50 lines the permeation passage. A ring of six negatively charged E43 in each of the Cx46 connexons showed much more negative pore surface electrostatic potential attracting divalent cations such as Mg^{2+} (Fig. 3B), whereas in Cx50 connexon a ring of six non-charged F43 produced a neutral pore surface electrostatic potential unlikely to attract Mg^{2+} at this position (Fig. 3B). Based on these structural insights and the equivalent residue involvement in Ca^{2+}-binding in Cx26 GJ, we hypothesize that Cx46 E43 is one of several residues involved in Mg^{2+}-binding in Cx46 GJ and a missense mutation on this residue, E43F in Cx46, could reduce the Mg^{2+} modulation at this site. Reversely, a missense mutant in Cx50, F43E, could increase the pore surface negative electrostatic potential to attract Mg^{2+} to enhance Mg^{2+} modulation.

Our experimental results showed that expressing Cx46 E43F formed functional GJs with a slope γ_j of 160.7 ± 2.9 pS (Fig. 4, n = 4) in Mg^{2+}-free intracellular solution, which was reduced to 144 ± 5.2 pS (n = 5, $^{*}P$ = 0.036) when 5 mmol/L Mg^{2+} was included in the ICS (Fig. 4). Cx50 F43E was also formed functional GJs with a slope γ_j of 226 ± 8.3 pS (Fig. 4, n = 5) in Mg^{2+}-free ICS. However, the channel rarely stayed at the fully open state for any extended period (Fig. 4). When recording with ICS containing 5 mmol/L Mg^{2+}, no functional GJs could be identified, which could be due to the Cx50 F43E GJ showing an increased sensitivity to Mg^{2+} binding to promote GJ channel closure.

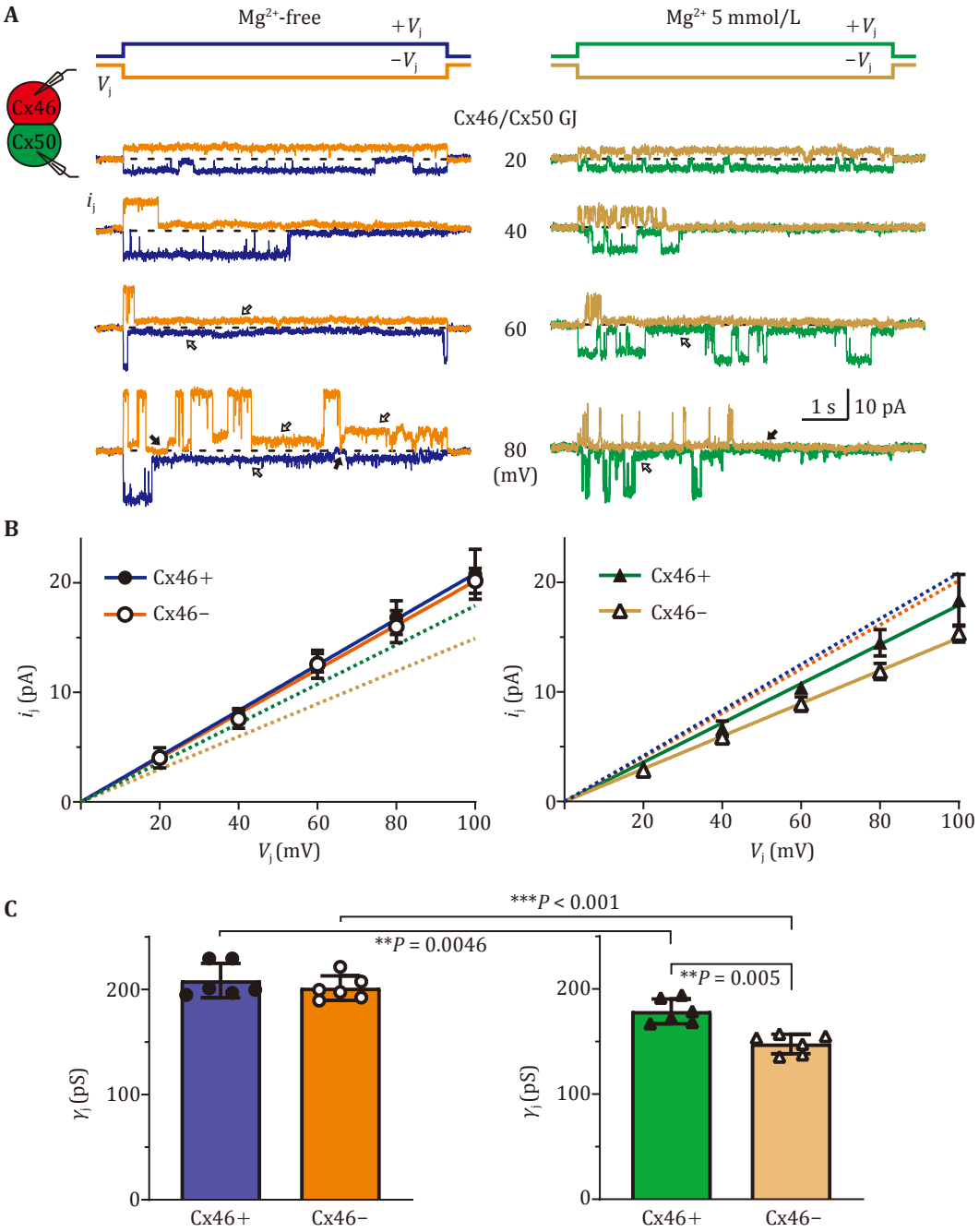

Fig. 1 Single channel properties of heterotypic Cx46/Cx50 GJ in the absence and presence of intracellular Mg^{2+}. **A** Dual whole cell patch clamp technique was used to measure single gap junction channel current (i_j) in response to the indicated V_j in heterotypic N2A cell pairs expressing sheep Cx46 in one (with untagged reporter DsRed) and sheep Cx50 in the other of the cell pair (with untagged reporter GFP). In the absence of intracellular Mg^{2+} (Mg^{2+}-free), the absolute i_js at the main conducting state were increased proportionally to the absolute V_js at both $+V_j$ (purple color) and $-V_j$ (orange color) polarities. Transitions from the main conducting state to the residue conducting state (open arrows) or fully closed state (filled arrow) could be observed especially on the i_js induced by ±40 or higher V_js. The i_js in the presence of 5 mmol/L Mg^{2+} were slightly lower in the amplitude for both $+V_j$ (in green color) and $-V_j$s (in brown color). **B** Main conducting state i_js were plotted against the V_j for each V_j polarity in the absence and presence of Mg^{2+}. Linear regressions of the i_j–V_j plots were used to obtain slope single channel conductance (γ_j) and the regression lines showed in different colors in the absence of Mg^{2+} (Cx46+ shown in purple and Cx46– shown in orange color) and the presence of 5 mmol/L Mg^{2+} (Cx46+ shown in green and Cx46– shown in brown color). The dotted lines were included to highlight the differences in slope γ_js. **C** Bar graphs illustrate the average γ_j for heterotypic Cx46/Cx50 GJ at different V_j polarities as indicated. The γ_js in the presence of 5 mmol/L Mg^{2+} displayed a statistical difference between Cx46+ and Cx46– (**P < 0.01). The γ_js of Cx46+ and Cx46– in the presence of 5 mmol/L Mg^{2+} were lower than their corresponding γ_js in the absence of Mg^{2+}

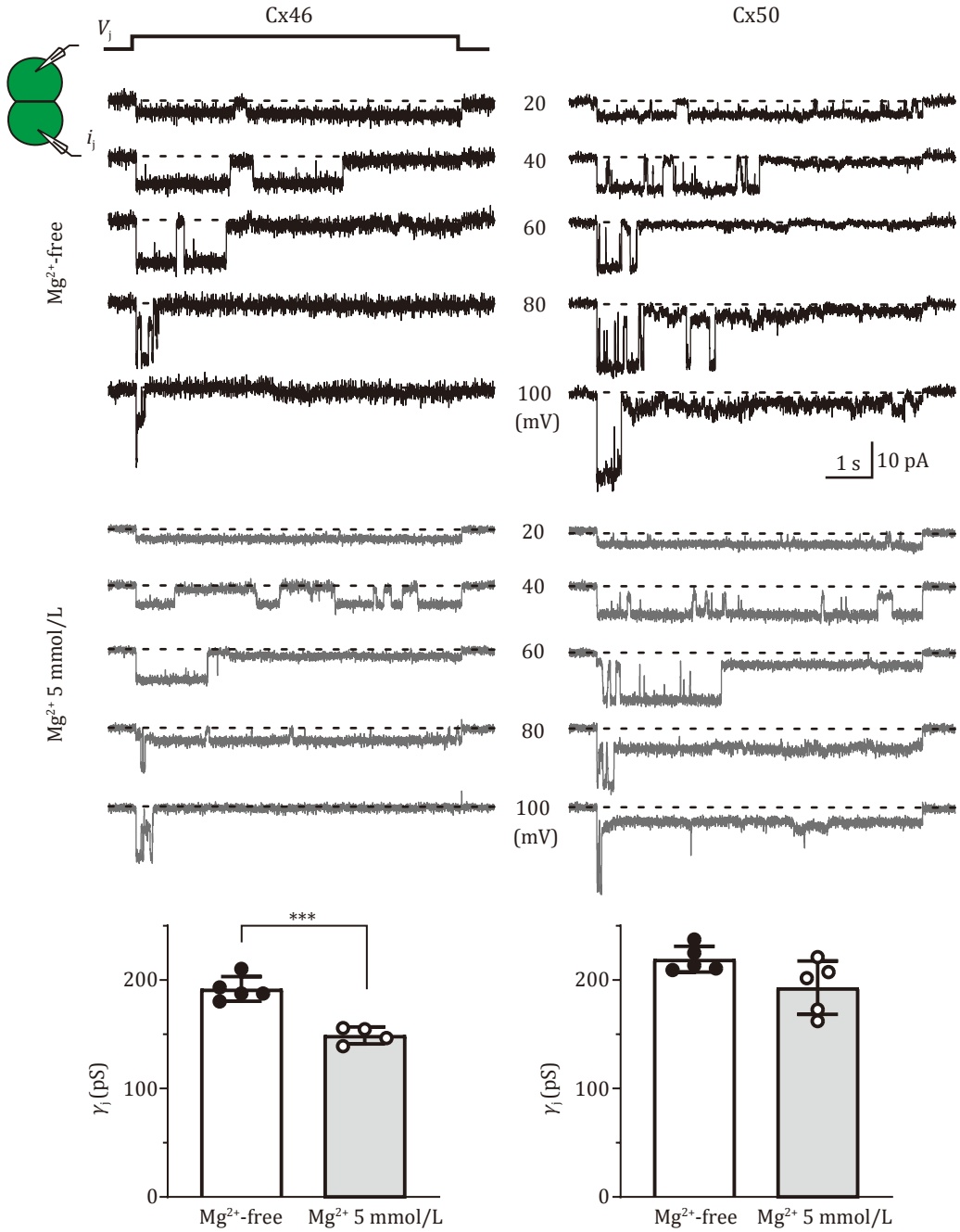

Fig. 2 Homotypic Cx46 and Cx50 GJs showed different sensitivity to intracellular Mg^{2+}. Unitary transjunctional currents (i_js) recorded from cell pairs expressing Cx46 (left panels) or Cx50 (right panels) in the absence (Mg^{2+} free, black traces) or presence (5 mmol/L Mg^{2+}, grey traces) of intracellular Mg^{2+} to different V_j pulses. The average slope γ_js of Cx46 and Cx50 GJs were plotted as bar graphs in the absence (open bars) and presence (grey bars) of 5 mmol/L Mg^{2+} as indicated. Statistical significance is indicated (***$P < 0.001$)

DISCUSSION

The present study identified an intracellular Mg^{2+} concentration dependent rectification of heterotypic Cx46/Cx50 GJs at individual channel levels. Specifically, the single channel conductance (γ_j) of Cx46/Cx50 GJ was significantly higher when the Cx46 cell was positive (defined as Cx46+) than that when the Cx46 cell was negative (Cx46–) with respect to the Cx50 cell in the intracellular solution containing 5 mmol/L Mg^{2+}, but in Mg^{2+}-free intracellular solution the γ_js of Cx46+ and Cx46– were larger and no difference was observed

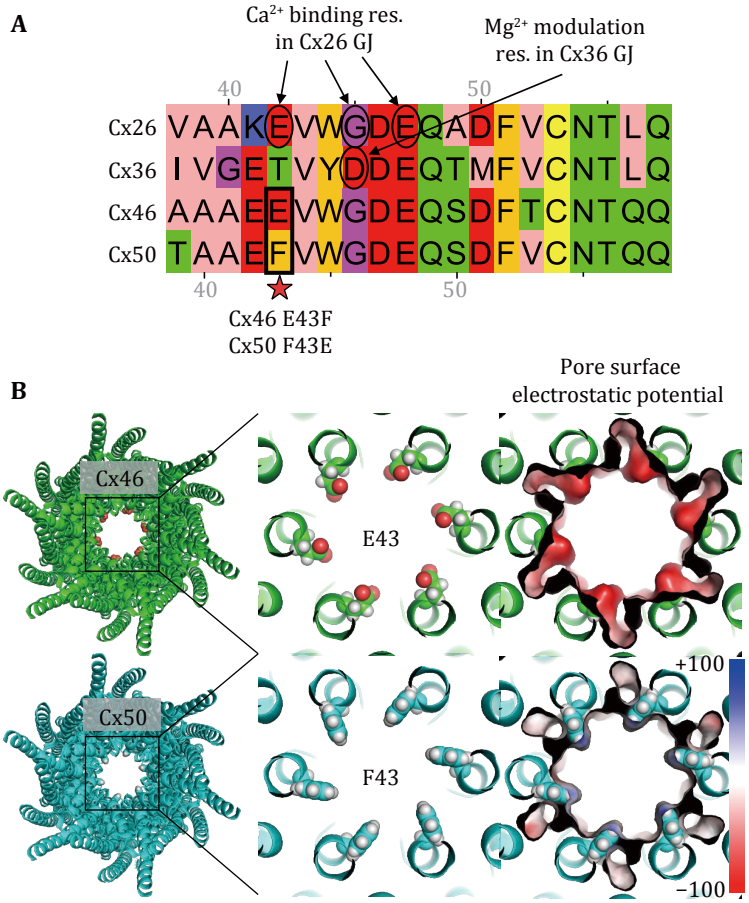

Fig. 3 Sequence alignment and possible residues involved in divalent cation binding in selected connexins. **A** Protein sequence alignment of human Cx26, Cx36, and sheep Cx46 and Cx50 near the border between the first transmembrane (M1) domain and the first extracellular (E1) domain. Ca^{2+}-binding residues in Cx26 and the key residue for Mg^{2+}-dependent modulation in Cx36 are indicated by circles and arrows. The residue numbering on the top follows that of Cx26 and the residue numbering at the bottom follows those of Cx46 and Cx50. Residues at the 43rd position of Cx46 and Cx50 are different (indicated by a rectangle box) and our designed variants are indicated below the alignment. **B** Structure models of Cx46 and Cx50 GJs (left panels), based on 7JKC and 7JJP (Flores *et al.* 2020), respectively, to show the sidechain of Cx46 E43 and Cx50 F43 are lining the pore (zoomed in view middle panels). The Cx46 E43 vacuum pore surface electrostatic potential showed stronger negative potential (red) than those of Cx50 F43 (mostly white with slightly blue, right panels)

between them. Elevation of [Mg^{2+}]$_i$ from zero to 5 mmol/L showed a significant reduction in the γ_j of homotypic Cx46 GJ with little change in the γ_j of homotypic Cx50 GJ. The [Mg^{2+}]$_i$-dependent reduction in Cx46 γ_j was likely due to the E43 of Cx46, as Cx46 E43F showed a reduced [Mg^{2+}]$_i$-modulation in γ_j. Unfortunately, we could not study the [Mg^{2+}]$_i$-modulation on Cx50 F43E as the GJ main open state became very unstable in the Mg^{2+}-free intracellular solution and no functional GJs could be formed in the presence of 5 mmol/L Mg^{2+}. Our study revealed that [Mg^{2+}]$_i$ could modulate the γ_j of Cx46 and Cx50 GJs differently leading to [Mg^{2+}]$_i$-dependent rectification of heterotypic Cx46/Cx50 GJ. Variation in intracellular Mg^{2+} concentrations under physiological and pathological conditions could regulate the γ_js of homotypic Cx46, heterotypic Cx46/Cx50, and possibly other GJs to fine tune intercellular communication in the lens and other tissues.

The underlying mechanism of how [Mg^{2+}]$_i$ could modulate Cx46/Cx50 GJ channel rectification is not clear. A previous study showed that the rectification of a heterotypic Cx26/Cx32 GJ channel was due to their differences in ion selectivity of the component hemichannels (Suchyna *et al.* 1999), *i.e.*, Cx26 GJ showed a strong cation preference while Cx32 GJ did not. When Cx26 and Cx32 hemichannels connected in

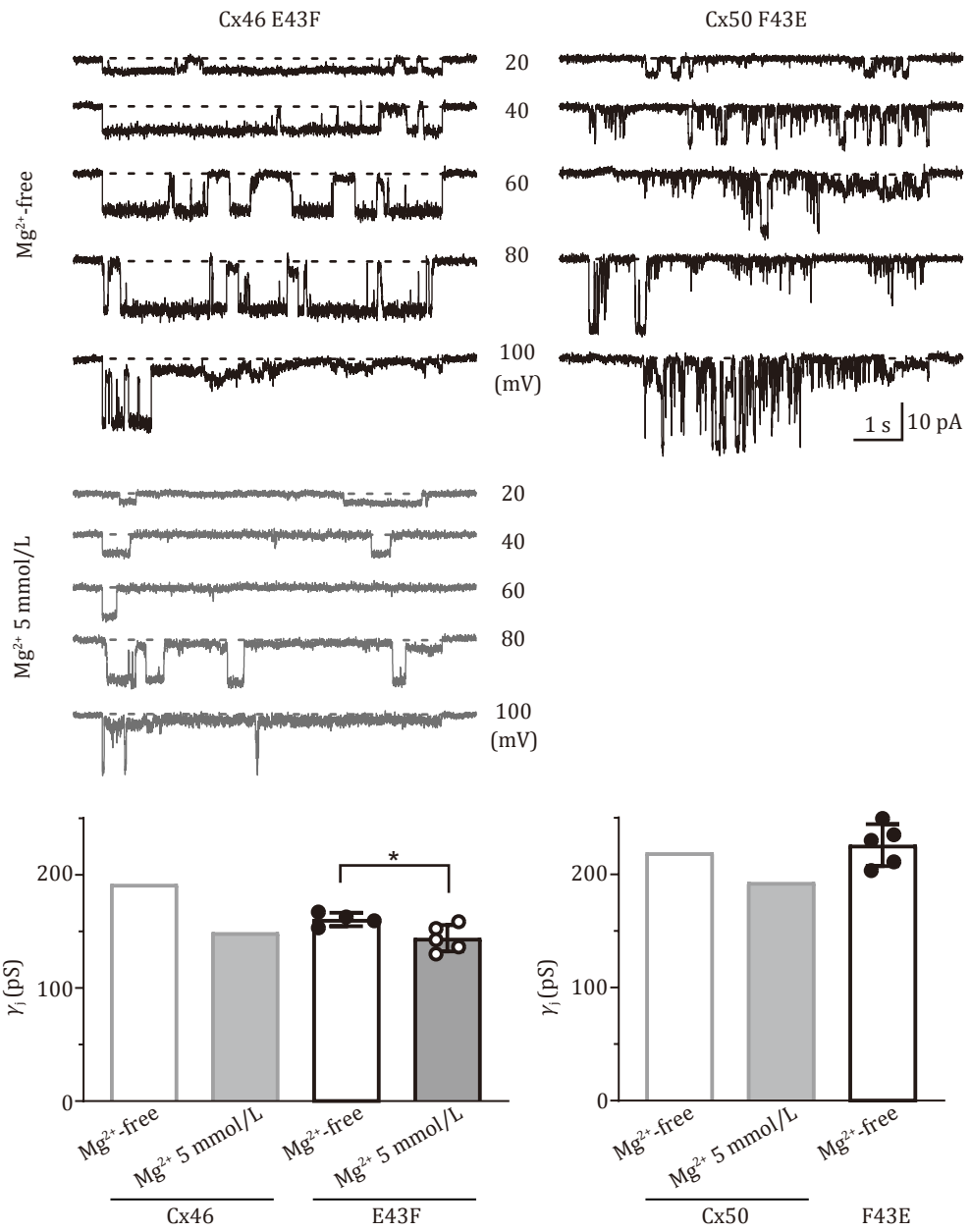

Fig. 4 Cx46 E43F showed an apparently lower percentage block by $[Mg^{2+}]_i$ compared to wildtype Cx46. Representative unitary transjunctional currents (i_js) recorded from cell pairs expressing Cx46 E43F (left top panel) or Cx50 F43E (right top panel) in the absence (Mg^{2+} free, black traces) or presence (5 mmol/L Mg^{2+}, middle panel with grey traces) of intracellular Mg^{2+} to different V_j pulses. In the presence of 5 mmol/L Mg^{2+} in the ICS, the Cx50 F43E failed to form any function GJs. The average slope γ_js of Cx46 E43F and Cx50 E43F GJs were plotted as bar graphs in the absence (open bars) and presence (grey bar) of 5 mmol/L Mg^{2+} as indicated. For easier comparison, the average slope γ_j of Cx46 and Cx50 GJs in the absence (Mg^{2+}-free) and the presence of 5 mmol/L Mg^{2+} are included in these bar graphs (from Fig. 2 with grey outlines). Statistical significance is indicated (*P = 0.036). Data points represent the number of cell pairs

series forming a GJ channel, the availability of cations and anions in different parts of the heterotypic GJ pore were different leading to current rectification (Suchyna *et al.* 1999). In the case of Cx46 and Cx50 GJs, the permeation ions showed cation preference for both GJs (Trexler *et al.* 1996; Srinivas *et al.* 1999; Sakai *et al.* 2003; Tong *et al.* 2014) and our measured γ_j of heterotypic Cx46/Cx50 GJ showed little difference with different V_j in the absence of Mg^{2+}. However, when 5 mmol/L Mg^{2+} is added into the intracellular solution, we believe that one or more Mg^{2+} can bind to the channel pore surface where negatively charged residues are

enriched, such as near the border of M1–E1 domains (Fig. 3). As Cx46 is predicted to have one additional negatively charged residue (E43, amplified into six in a hexameric Cx46 hemichannel) than Cx50, it is therefore more likely to interact with Mg^{2+} whenever intracellular Mg^{2+} is available. The interaction between Mg^{2+} and the pore lining residues could cause changes in local electrostatic properties, which in turn could alter the local concentrations of cations and anions to change the channel cation/anion preference on the Cx46 half of the heterotypic Cx46/Cx50 GJ, leading to rectification as observed. Consistent with this model, we did observe a significant reduction in the γ_j (22%) of wild-type Cx46 GJ in the presence of $[Mg^{2+}]_i$, while little change in the γ_j of Cx50 GJ was observed. In addition, Cx46 E43F variant GJ is predicted to have a decreased negative electrostatic potential at the M1–E1 border region and its GJ showed a decreased γ_j reduction (10%) by $[Mg^{2+}]_i$. Additional experiments with enlarged cations or anions to directly test the cation/anion preference for homotypic Cx46, its variant E43F, and Cx50 GJs would be required to reveal if these GJs' cation/anion preferences and γ_js are different with different sized permeation ions.

Most of the intracellular Mg^{2+} ions are in bound form with ATP or enzymes as a co-factor, the free Mg^{2+} concentration was estimated to be only a small fraction of the total intracellular Mg^{2+} (Romani and Scarpa 2000; Maguire and Cowan 2002). This is also the case for our experiments described above. We included 5 mmol/L MgATP in the patch pipette solution and the estimated free $[Mg^{2+}]_i$ is ~8 times lower (0.6 mmol/L) according to an online program (Maxchelator) with our patch pipette solution (Patton *et al.* 2004). We believe that this estimation is likely an underestimation of $[Mg^{2+}]_i$ as ATP is not stable in solutions and is likely partially hydrolyzed into ADP and AMP, both of which showed a lower affinity in binding Mg^{2+} than ATP. This free $[Mg^{2+}]_i$ is well within the range of estimated free concentrations for Mg^{2+} in cytosols for most tissues (0.2–3.5 mmol/L) (London 1991; Chen *et al.* 2003). It is interesting to note that at this free $[Mg^{2+}]_i$, we did not observe a statistically significant decrease in the γ_js of Cx50 GJ as we reported earlier (Tejada *et al.* 2018). We believe that several reasons could be responsible for this apparent difference. (1) We did not include any ATP in the patch pipette solution in our previous study, therefore using 1 or 3 mmol/L $MgCl_2$ in the patch pipette solution, the Maxchelator estimated free $[Mg^{2+}]_i$ are around 0.7 or 2.1 mmol/L, respectively. These free concentrations of Mg^{2+} are actually higher than simply including 5 mmol/L MgATP. (2) Our previous study used mouse Cx50 which showed a sequence identity of 87% from sheep Cx50 (the one we used for the current study). With 13% different residues, the sheep GJ structure could be slightly different leading to some differences in Mg^{2+}-dependent modulation on γ_j. (3) We could not rule out other additional differences in handling solutions by different researchers for these patch clamp experiments. In addition to modulating the γ_j, higher free $[Mg^{2+}]_i$ (in the 1–10 mmol/L range) was previously shown to be able to affect V_j-gating properties in Cx36, Cx43, and Cx47 GJs (Palacios-Prado *et al.* 2013). In contrast to these findings, our previous study on mouse Cx50 failed to observe any V_j-gating property change at 3 mmol/L Mg^{2+} without any added ATP (Tejada *et al.* 2018). It is not clear if the V_j-gating properties of Cx46 GJs could be modulated by higher $[Mg^{2+}]_i$, this needs to be tested experimentally in future studies.

The heterotypic Cx46/Cx50 GJ channel displayed rectification in the presence of $[Mg^{2+}]_i$, indicating that these heterotypic GJs could play a role in facilitating directional movement of ions. GJs are large pores able to not only permeate ions but also larger organic substrates up to one kilodalton in molecular weight. The rectification of ionic currents in the heterotypic GJ channels could be amplified to promote directional permeation of larger organic substrates, such as nutrients, metabolites, and signaling molecules. Regulating the directional permeation of these molecules through heterotypic GJ channels could be important for GJ-dependent lens circulation to keep this avascular organ transparent. Currently, it is not clear how Cx46 and Cx50 are assembled into different types of heteromeric and/or heterotypic GJs. Heterotypic Cx46/Cx50 GJ might not be the dominant GJ type in lens fiber cells for directional circulation. Whether complex heteromeric GJs formed by a mixture of Cx46 and Cx50 also display rectification properties will require properly designed experiments to demonstrate.

Elevation of either $[Ca^{2+}]_i$ or $[Mg^{2+}]_i$ has been shown to eliminate/reduce GJ function in cells expressing different connexins (Loewenstein *et al.* 1967; Oliveira-Castro and Loewenstein 1971; Noma and Tsuboi 1987; Peracchia *et al.* 2000; Peracchia 2004; Chen *et al.* 2011; Palacios-Prado *et al.* 2013). However, some key differences are noted between $[Ca^{2+}]_i$ and $[Mg^{2+}]_i$ modulations on GJs. (1) The concentrations of intracellular Ca^{2+} and Mg^{2+} are quite different in tissue cells under physiological conditions. The endogenous $[Ca^{2+}]_i$ is in the tens to hundreds of nano molar (nmol/L) range and $[Mg^{2+}]_i$ is in the sub- or low-millimolar range (Grubbs 2002). So the $[Mg^{2+}]_i$ is at least 1000 times higher than $[Ca^{2+}]_i$, to affect the GJ channel function. (2) Elevation of $[Ca^{2+}]_i$ to micro molars often leads to the elimination of

GJ coupling (Peracchia 2004; Chen *et al.* 2011; Zou *et al.* 2014), while the increase in $[Mg^{2+}]_i$ to milli molars showed a significantly reduced GJ coupling, but not elimination (Palacios-Prado *et al.* 2013). Previous works indicated that 5 mmol/L free $[Mg^{2+}]_i$ reduce coupling conductance of GJs of Cx26, Cx32, Cx36, Cx43, Cx45, and Cx47 (Palacios-Prado *et al.* 2013; Palacios-Prado *et al.* 2014). It is not clear whether this reduction is due to a decrease in GJ channel open probability, γ_j, or both. Our previous works showed that $[Mg^{2+}]_i$ (without any added ATP in patch pipette) dose dependently reduced γ_j of Cx50 (Tejada *et al.* 2018) and now we showed that Cx46 γ_j was more sensitive to $[Mg^{2+}]_i$ (together with ATP) than that of Cx50 γ_j leading to the rectification of heterotypic Cx46/Cx50 γ_j. (3) The underlying molecular/structural mechanisms of how Ca^{2+} modulates GJs are not fully clear. Depending on the $[Ca^{2+}]_i$, Ca^{2+} could have an indirect effect on GJ via calmodulin (Peracchia 2004; Dodd *et al.* 2008; Chen *et al.* 2011; Zou *et al.* 2014) without changing γ_j in Cx50 GJ (Chen *et al.* 2011). Another possibility is that intracellular Ca^{2+} could directly bind to the GJ pore lining residues to block/reduce ion permeation. This idea was supported by a structural study with a total of 12 Ca^{2+}-binding sites mapped onto residues (E42, G45, and E47) at the border of M1–E1 domains in the Cx26 subunit (Bennett *et al.* 2016). Binding one or more Ca^{2+} in a GJ could drastically change the pore electrostatic properties (Bennett *et al.* 2016). Another study showed evidence that Ca^{2+} binds to D50 and E47 of Cx26 to gate un-apposed hemichannel to a closed state (Lopez *et al.* 2016). The region of the M1 and E1 border is highly conserved with a cluster of negatively charged residues, which could serve to bind divalent cations including Ca^{2+} and possibly Mg^{2+}. Supporting this divalent cation binding model, the $[Mg^{2+}]_i$-dependent increase in coupling conductance of Cx36 GJ was also mapped to a residue in this M1–E1 region (Palacios-Prado *et al.* 2014). In addition, Cx37 and Cx50 GJ channels showed a decrease in γ_j with elevation of $[Mg^{2+}]_i$ (Banach *et al.* 2000; Tejada *et al.* 2018). The results from our current study are consistent with a possible binding of Mg^{2+} to this region of Cx46 and Cx50 GJ to reduce differentially the rate of ion permeation (or γ_j). Molecular dynamic studies showed that divalent cations showed an increased dwell time at residues (E47 and D50) at the M1–E1 region in Cx26 (Zonta *et al.* 2014; Lopez *et al.* 2016). Structural and molecular dynamic studies in the presence of Mg^{2+} would help to further reveal the mechanisms of how Mg^{2+} modulates these lens GJs.

The single channel conductance (γ_j) differences of Cx46/Cx50 GJ channels in our study in the presence of Mg^{2+} are different from those reported previously (Hopperstad *et al.* 2000). We do not have a simple explanation, but possibilities could include inter-species differences between sheep connexins (from current study) vs. the rodent connexins (used in the previous study), differences in patch pipette solution, and/or differences in conventions and patch clamp handling procedures *etc*. This should be verified in future studies, ideally from the same laboratory.

Cx46, Cx50, and most of our designed Cx46 and Cx50 variants expressed well in GJ-deficient N2A cells and were able to form functional GJs as both single channel and macroscopic GJ currents were recorded. To optimize the yield of recording cell pairs with only 1–2 functional GJs, we lowered the replating time to as low as 30 minutes on the recording day. Even with this optimized condition, the yield of getting GJ single channel current was still very low (less than 10% of total recorded cell pairs). With this low yield, we could not test systematically for different doses of $[Mg^{2+}]_i$ to construct dose–inhibition curves for proper pharmacological analysis. The Cx50 F43E did show single channel currents but rarely stayed at the fully open state in the Mg^{2+}-free patch pipette solution. In the presence of 5 mmol/L $[Mg^{2+}]_i$, we could not record any functional GJs. Most likely the Cx50 F43E GJs stayed in a fully closed state and were unable to transition to a fully open state.

During the data collection of single heterotypic Cx46/Cx50 GJ currents, we also recorded many cell pairs with macroscopic GJ currents in response to different V_js. However, we noticed that the peak amplitude of macroscopic GJ currents was not stable and could not be used as a good representation of the single channel currents at the main conductance state, specifically the rectification property was not clear in these macroscopic GJ currents at different V_js. The main reason for this apparent discrepancy was that the peak macroscopic currents at the relatively high V_js (±60 to ±100 mV) were not very stable due to incomplete recovery from the previous V_j-induced V_j-gating (which pushed a lot of functional GJs into residue conductance or fully closed states and likely only a portion of these gated channels was recovered at the given inter pulse interval) as well as the differences in gating kinetics of GJ deactivation during the V_j pulse. We tried to increase the inter pulse interval to allow a longer time for improved recovery from deactivated GJ channels but failed to resolve the macroscopic current stability issue as sometimes the GJ currents 'run down' and/or are not stable during the prolonged period (*e.g.*, change in access for the whole recording and/or leak changes at the patch *etc*.). This is the reason we only focused on

quantitative analysis of single channel GJ currents at the main conductance state in this study, which is a much more reliable parameter for heterotypic GJ channels.

In conclusion, we showed that the elevation of intracellular Mg^{2+} to 5 mmol/L led to a differential reduction in the γ_js of Cx46 and Cx50 GJs. The relatively higher reduction in Cx46 γ_j than in Cx50 γ_j by Mg^{2+} caused rectification in the γ_j of heterotypic Cx46/Cx50 GJ.

METHOD

Plasmid construction

We used expression constructs (pIRES2) with an untagged fluorescent reporter gene, encoding either EGFP (pIRES2-EGFP) or DsRed (pIRES2-DsRed2). Sheep Cx50-IRES-GFP (also known as Cx49 or sCx50), sheep Cx46-IRES-GFP (also known as Cx44) and Cx46-IRES-DsRed were generated as previously described (Yue *et al.* 2021; Jaradat *et al.* 2022). Briefly, the cDNAs of Cx50 or Cx46 were synthesized and each of them was inserted into the expression vector at the restriction enzyme sites, XhoI and EcoRI (NorClone Biotech Laboratories, London, Ontario). These vectors were used as templates to generate point mutations, Cx46 E43F and Cx50 F43E, with the following primers:

Cx46 E43F: forward 5' GCC GCG GCC GAG TTC GTG TGG GGG GAT GAG 3' and reverse 5' CTC ATC CCC CCA CAC GAA CTC GGC CGC GGC 3'

Cx50 F43E: forward 5' GGT ACT GCT GCA GAC GAG GTG TGG GGG GAT GAG 3' and reverse 5' CTC ATC CCC CCA CAC CTC GTC TGC AGC AGT ACC 3'

Cell culture and transient transfection

Gap junction deficient neuroblastoma (N2A) cells (American Type Culture Collection, Manassas, VA) were cultured and grown in Dulbecco's modified Eagle's medium (DMEM) containing 4.5 g/L D-(+)-glucose, 584 mg/L L-glutamine (4 mmol/L), 110 mg/L sodium pyruvate, 10% fetal bovine serum (FBS), 1% penicillin (100 units/mL), and 1% streptomycin (100 µg/mL or 172 µmol/L), in an incubator with 5% CO_2 at 37 °C (Sun *et al.* 2013). N2A cells at ~60% confluence were transfected with 1.0 µg of a cDNA construct and 2 µL of X-tremeGENE HP DNA transfection reagent (Roche Diagnostics GmbH, Indianapolis, IN, USA) in a regular medium overnight. Next, morning the transfected cells were replated onto coverslips for 0.5–1.5 h prior to recording. For heterotypic GJs, cells transfected with Cx46-IRES-DsRed were mixed with cells transfected with Cx50-IRES-EGFP before replating onto coverslips for 0.5–1.5 h. Cell pairs with one red and the other green were selected for dual patch clamp recording.

Electrophysiological recording

Glass coverslips with transfected cells were placed into a recording chamber one at a time on an inverted fluorescent microscope (DMIRB, Leica). The chamber was filled with extracellular solution (ECS) at room temperature (21–24 °C). The ECS contained (in mmol/L): 135 NaCl, 2 CsCl, 2 $CaCl_2$, 1 $MgCl_2$, 1 $BaCl_2$, 10 HEPES, 5 KCl, 5 D-(+)-glucose, 2 Sodium pyruvate, pH 7.4 (adjusted with 1 mol/L NaOH), and with an osmolarity of 310–320 mOsm. Patch pipettes were pulled using a micropipette puller (PC-100, Narishige International USA Inc., Amityville, NY, USA) and filled with intracellular solution (ICS). The Mg^{2+}-free ICS contains (in mmol/L): 130 CsCl, 10 EGTA, 0.5 $CaCl_2$, 5 Na_2ATP, and 10 HEPES, adjusted to pH 7.2 with 1 mol/L CsOH, and with an osmolarity of 290–300 mOsm. For Mg^{2+} containing ICS, 5 mmol/L MgATP was used to replace Na_2ATP. Isolated heterotypic red/green cell pairs (GFP and DsRed reporter expressing cell pairs) were selected to study heterotypic Cx46/Cx50 GJs. For homotypic GJ studies, isolated GFP expressing cell pairs were selected.

Single channel recording and analysis

After whole cell recording was established, both cells were initially voltage clamped at 0 mV with Axopatch 200B amplifiers (Molecular Devices, Sunnyvale, CA, USA). A series of voltage pulses (±20 to ±100 mV with 20 mV increment and 7 s duration) were administered to one of the cells to establish transjunctional voltage (V_j). The other cell was held at 0 mV to record unitary transjunctional current (i_j). The i_j was low-pass filtered (cut-off frequency at 1 kHz) at the amplifier, digitized via an AD/DA converter at a sampling rate of 10 kHz (Digidata 1322A, Molecular Devices, Sunnyvale, CA, USA), and recorded with Clampex9.2 software (pClamp9.2, Molecular Devices, Sunnyvale, CA, USA).

Single gap junctional currents (i_js) could be observed in cell pairs with few active channels. The i_js were further filtered using a low-pass Gaussian filter at 200 Hz in Clampfit 9.2 for measuring current amplitude and display in figures. The amplitude i_j values for the fully open state at different V_js were measured by either fitting Gaussian functions on all-point current amplitude histograms or directly reading manually in

Clampfit. For homotypic Cx46, Cx50, and their variant GJs, the i_j values of the same cell pair with two V_j polarity were averaged and then plotted with each tested V_js to generate i_j–V_j plot for each cell pair. Linear regression of the i_j–V_j plot for each cell pair was used to estimate slope unitary GJ channel conductance (also known as slope single channel conductance, γ_j). The slope γ_js of different cell pairs were averaged and presented as bar graphs. For heterotypic Cx46 / Cx50 GJs, two V_j polarities were individually defined and analyzed. When the Cx46 expressing cell with $+V_j$s (or the Cx50 expressing cell with $-V_j$s), the V_j polarity was defined as Cx46+. Reversely, when the Cx46 expressing cell with $-V_j$s (or the Cx50 expressing cell with $+V_j$s), the V_j polarity was defined as Cx46–. The i_js of both Cx46+ and Cx46– polarities were analyzed separately and i_j–V_j plots were generated to obtain slope γ_js for each of these polarities. Slope γ_js were averaged and plotted as bar graphs for statistical comparison.

Statistical analysis

Data in i_j–V_j plots and bar graphs represent mean ± SEM. Paired Student *t*-test was used to compare slope γ_js of Cx46+ and Cx46– V_j polarity in heterotypic Cx46/Cx50 GJs. The unpaired *t*-test was used to compare γ_j values of homotypic GJs of different connexins, their variants, and/or under different $[Mg^{2+}]_i$ concentrations. Statistical significance is indicated with the asterisks on the graphs for group comparisons (*P < 0.05; **P < 0.01; or ***P < 0.001).

Abbreviations

Cx46	Connexin46
Cx50	Connexin50
GJ	Gap junction
i_j	Unitary gap junctional current
γ_j	Single gap junction channel conductance
V_j	Transjunctional voltage

Acknowledgements This work was supported by Natural Sciences and Engineering Research Council of Canada (288241 to D.B.).

Author contributions Design and conducting dual patch clamp experiments, data analyzing, generating plots H.C. Project design, obtain funding support, manuscript writing and revision, and supervision D.B. Both authors have read and agreed to the submitted version of the manuscript.

Data availability All data in this study are available from the corresponding author upon request.

Compliance with Ethical Standards

Conflict of interest Honghong Chen and Donglin Bai declare that they have no conflict of interest.

Human and animal rights and informed consent This article does not contain any studies with human or animal subjects performed by any of the authors.

References

Abrams CK, Peinado A, Mahmoud R, Bocarsly M, Zhang H, Chang P, Botello-Smith WM, Freidin MM, Luo Y (2018) Alterations at Arg(76) of human connexin 46, a residue associated with cataract formation, cause loss of gap junction formation but preserve hemichannel function. Am J Physiol Cell Physiol 315: C623–c635

Bai D, Wang J, Li T, Chan R, Atalla M, Chen RC, Khazaneh MT, An RJ, Stathopulos PB (2021) Differential domain distribution of gnomAD- and disease-linked connexin missense variants. Int J Mol Sci 22: 22(15): 7832. https://doi.org/10.3390/ijms22157832

Banach K, Ramanan SV, Brink PR (2000) The influence of surface charges on the conductance of the human connexin37 gap junction channel. Biophys J 78: 752–760

Bargiello T, Brink P. (2009). Voltage-gating mechanisms of connexin channels. In: Connexins: a guide. Harris AL, Locke D (Ed). pp. 103-128. Clifton, New Jersey: Humana Press

Bennett BC, Purdy MD, Baker KA, Acharya C, McIntire WE, Stevens RC, Zhang Q, Harris AL, Abagyan R, Yeager M (2016) An electrostatic mechanism for Ca^{2+}-mediated regulation of gap junction channels. Nat Commun 12: 7: 8770. https://doi.org/10.1038/ncomms9770

Berthoud VM, Gao J, Minogue PJ, Jara O, Mathias RT, Beyer EC (2019) The connexin50D47A mutant causes cataracts by calcium precipitation. Invest Ophthalmol Vis Sci 60: 2336–2346

Beyer EC, Ebihara L, Berthoud VM (2013) Connexin mutants and cataracts. Front Pharmacol 4: 43. https://doi.org/10.3389/fphar.2013.0004

Beyer EC, Kistler J, Paul DL, Goodenough DA (1989) Antisera directed against connexin43 peptides react with a 43-kD protein localized to gap junctions in myocardium and other tissues. J Cell Biol 108: 595–605

Bukauskas FF, Verselis VK (2004) Gap junction channel gating. Biochim Biophys Acta 1662: 42–60

Ceroni F, Aguilera-Garcia D, Chassaing N, Bax DA, Blanco-Kelly F,

Ramos P, Tarilonte M, Villaverde C, da Silva LRJ, Ballesta-Martinez MJ, Sanchez-Soler MJ, Holt RJ, Cooper-Charles L, Bruty J, Wallis Y, McMullan D, Hoffman J, Bunyan D, Stewart A, Stewart H, Lachlan K, Fryer A, McKay V, Roume J, Dureau P, Saggar A, Griffiths M, Calvas P, Ayuso C, Corton M, Ragge NK, Study DDD (2019) New GJA8 variants and phenotypes highlight its critical role in a broad spectrum of eye anomalies. Hum Genet 138: 1027–1042

Chen C, Nakatani K, Koutalos Y (2003) Free magnesium concentration in salamander photoreceptor outer segments. J Physiol 553: 125–135

Chen Y, Zhou Y, Lin X, Wong HC, Xu Q, Jiang J, Wang S, Lurtz MM, Louis CF, Veenstra RD, Yang JJ (2011) Molecular interaction and functional regulation of connexin50 gap junctions by calmodulin. Biochem J 435: 711–722

Dodd R, Peracchia C, Stolady D, Török K (2008) Calmodulin association with connexin32-derived peptides suggests trans-domain interaction in chemical gating of gap junction channels. J Biol Chem 283: 26911–26920

Flores JA, Haddad BG, Dolan KA, Myers JB, Yoshioka CC, Copperman J, Zuckerman DM, Reichow SL (2020) Connexin-46/50 in a dynamic lipid environment resolved by CryoEM at 1.9 Å. Nat Commun 11(1): 4331. https://doi.org/10.1038/s41467-020-18120-5

Gong X, Li E, Klier G, Huang Q, Wu Y, Lei H, Kumar NM, Horwitz J, Gilula NB (1997) Disruption of alpha3 connexin gene leads to proteolysis and cataractogenesis in mice. Cell 91: 833–843

Goodenough DA, Paul DL (2009) Gap junctions. Cold Spring Harb Perspect Biol 1(1): a002576. https://doi.org/10.1101/cshperspect.a002576

Grubbs RD (2002) Intracellular magnesium and magnesium buffering. Biometals 15: 251–259

Hopperstad MG, Srinivas M, Spray DC (2000) Properties of gap junction channels formed by Cx46 alone and in combination with Cx50. Biophys J 79: 1954–1966

Jaradat R, Li X, Chen H, Stathopulos PB, Bai D (2022) The hydrophobic residues in amino terminal domains of Cx46 and Cx50 are important for their gap junction channel ion permeation and gating. Int J Mol Sci 23(19): 11605. https://doi.org/10.3390/ijms231911605

Jiang JX, Goodenough DA (1996) Heteromeric connexons in lens gap junction channels. Proc Natl Acad Sci USA 93: 1287–1291

Konig N, Zampighi GA (1995) Purification of bovine lens cell-to-cell channels composed of connexin44 and connexin50. J Cell Sci 108 (Pt 9): 3091-3098

Kumar NM, Gilula NB (1996) The gap junction communication channel. Cell 84: 381–388

Lampe PD, Lau AF (2004) The effects of connexin phosphorylation on gap junctional communication. Int J Biochem Cell Biol 36: 1171–1186

Li T, Chen H, Li X, Stathopulos PB, Bai D (2023) Inherited disease-linked arginine76/75 mutants in Cx50 and Cx45 showed impaired homotypic and heterotypic gap junction function, but not Cx43. Biochem J 480: 1051–1077

Loewenstein WR, Nakas M, Socolar SJ (1967) Junctional membrane uncoupling. Permeability transformations at a cell membrane junction. J Gen Physiol 50: 1865–1891

London RE (1991) Methods for measurement of intracellular magnesium: NMR and fluorescence. Annu Rev Physiol 53: 241–258

Lopez W, Ramachandran J, Alsamarah A, Luo Y, Harris AL, Contreras JE (2016) Mechanism of gating by calcium in connexin hemichannels. Proc Natl Acad Sci USA 113: E7986–e7995

Maguire ME, Cowan JA (2002) Magnesium chemistry and biochemistry. Biometals 15: 203–210

Mathias RT, White TW, Gong X (2010) Lens gap junctions in growth, differentiation, and homeostasis. Physiol Rev 90: 179–206

Matsuda H, Kurata Y, Oka C, Matsuoka S, Noma A (2010) Magnesium gating of cardiac gap junction channels. Prog Biophys Mol Biol 103: 102–110

Myers JB, Haddad BG, O'Neill SE, Chorev DS, Yoshioka CC, Robinson CV, Zuckerman DM, Reichow SL (2018) Structure of native lens connexin 46/50 intercellular channels by cryo-EM. Nature 564: 372–377

Noma A, Tsuboi N (1987) Dependence of junctional conductance on proton, calcium and magnesium ions in cardiac paired cells of guinea-pig. J Physiol 382: 193–211

Oliveira-Castro GM, Loewenstein WR (1971) Junctional membrane permeability: effects of divalent cations. J Membr Biol 5: 51–77

Pal JD, Berthoud VM, Beyer EC, Mackay D, Shiels A, Ebihara L (1999) Molecular mechanism underlying a Cx50-linked congenital cataract. Am J Physiol 276: C1443–1446

Palacios-Prado N, Chapuis S, Panjkovich A, Fregeac J, Nagy JI, Bukauskas FF (2014) Molecular determinants of magnesium-dependent synaptic plasticity at electrical synapses formed by connexin36. Nat Commun 5: 4667. https://doi.org/10.1038/ncomms5667

Palacios-Prado N, Hoge G, Marandykina A, Rimkute L, Chapuis S, Paulauskas N, Skeberdis VA, O'Brien J, Pereda AE, Bennett MV, Bukauskas FF (2013) Intracellular magnesium-dependent modulation of gap junction channels formed by neuronal connexin36. J Neurosci 33: 4741–4753

Patton C, Thompson S, Epel D (2004) Some precautions in using chelators to buffer metals in biological solutions. Cell Calcium 35: 427–431

Paul DL, Ebihara L, Takemoto LJ, Swenson KI, Goodenough DA (1991) Connexin46, a novel lens gap junction protein, induces voltage-gated currents in nonjunctional plasma membrane of Xenopus oocytes. J Cell Biol 115: 1077–1089

Peracchia C (2004) Chemical gating of gap junction channels: Roles of calcium, pH and calmodulin. Biochimica et Biophysica Acta (BBA) - Biomembranes 1662: 61–80

Peracchia C, Peracchia LL (1980) Gap junction dynamics: reversible effects of divalent cations. J Cell Biol 87: 708–718

Peracchia C, Wang XG, Peracchia LL (2000) Chemical gating of gap junction channels. Methods 20: 188–195

Romani AM, Scarpa A (2000) Regulation of cellular magnesium. Front Biosci 5: D720–734

Saez JC, Berthoud VM, Branes MC, Martinez AD, Beyer EC (2003) Plasma membrane channels formed by connexins: their regulation and functions. Physiol Rev 83: 1359–1400

Sakai R, Elfgang C, Vogel R, Willecke K, Weingart R (2003) The electrical behaviour of rat connexin46 gap junction channels expressed in transfected HeLa cells. Pflugers Arch 446: 714–727

Schadzek P, Schlingmann B, Schaarschmidt F, Lindner J, Koval M, Heisterkamp A, Preller M, Ngezahayo A (2016) The cataract related mutation N188T in human connexin46 (hCx46) revealed a critical role for residue N188 in the docking process of gap junction channels. Biochim Biophys Acta 1858: 57–66

Srinivas M, Costa M, Gao Y, Fort A, Fishman GI, Spray DC (1999) Voltage dependence of macroscopic and unitary currents of gap junction channels formed by mouse connexin50 expressed in rat neuroblastoma cells. J Physiol 517: 673–689

Suchyna TM, Nitsche JM, Chilton M, Harris AL, Veenstra RD, Nicholson BJ (1999) Different ionic selectivities for connexins 26 and 32 produce rectifying gap junction channels. Biophys J 77: 2968–2987

Sun Y, Yang YQ, Gong XQ, Wang XH, Li RG, Tan HW, Liu X, Fang WY, Bai D (2013) Novel germline GJA5/connexin40 mutations associated with lone atrial fibrillation impair gap junctional

intercellular communication. Hum Mutat 34: 603–609
Tejada MG, Sudhakar S, Kim NK, Aoyama H, Shilton BH, Bai D (2018) Variants with increased negative electrostatic potential in the Cx50 gap junction pore increased unitary channel conductance and magnesium modulation. Biochem J 475: 3315–3330
Tong JJ, Sohn BC, Lam A, Walters DE, Vertel BM, Ebihara L (2013) Properties of two cataract-associated mutations located in the NH2 terminus of connexin 46. Am J Physiol Cell Physiol 304: C823–832
Tong X, Aoyama H, Tsukihara T, Bai D (2014) Charge at the 46th residue of connexin 50 is crucial for the gap-junctional unitary conductance and transjunctional voltage-dependent gating. J Physiol 592: 5187–5202.
Trexler EB, Bennett MV, Bargiello TA, Verselis VK (1996) Voltage gating and permeation in a gap junction hemichannel. Proc Natl Acad Sci USA 93: 5836–5841
White TW, Bruzzone R, Goodenough DA, Paul DL (1992) Mouse Cx50, a functional member of the connexin family of gap junction proteins, is the lens fiber protein MP70. Mol Biol Cell 3: 711–720
White TW, Bruzzone R, Wolfram S, Paul DL, Goodenough DA (1994) Selective interactions among the multiple connexin proteins expressed in the vertebrate lens: the second extracellular domain is a determinant of compatibility between connexins. J Cell Biol 125: 879–892
White TW, Goodenough DA, Paul DL (1998) Targeted ablation of connexin50 in mice results in microphthalmia and zonular pulverulent cataracts. J Cell Biol 143: 815–825
Wong RS, Chen H, Li YX, Esseltine JL, Stathopulos PB, Bai D (2024) Human Cx50 Isoleucine177 prevents heterotypic docking and formation of functional gap junction channels with Cx43. Am J Physiol Cell Physiol 326: C414–C428
Xu X, Ebihara L (1999) Characterization of a mouse Cx50 mutation associated with the No2 mouse cataract. Invest Ophthalmol Vis Sci 40: 1844–1850
Yue B, Haddad BG, Khan U, Chen H, Atalla M, Zhang Z, Zuckerman DM, Reichow SL, Bai D (2021) Connexin 46 and connexin 50 gap junction channel properties are shaped by structural and dynamic features of their N-terminal domains. J Physiol 599: 3313–3335
Zonta F, Mammano F, Torsello M, Fortunati N, Orian L, Polimeno A (2014) Role of gamma carboxylated Glu47 in connexin 26 hemichannel regulation by extracellular Ca(2+): Insight from a local quantum chemistry study. Biochem Biophys Res Commun 445: 10–15
Zou J, Salarian M, Chen Y, Veenstra R, Louis CF, Yang JJ (2014) Gap junction regulation by calmodulin. FEBS Lett 588: 1430–1438

